

## Effect of a Continuous Feed on the Fluid-Dynamics of a Mechanically Stirred Tank

Antonio Busciglio<sup>a</sup>, Giuseppina Montante<sup>a</sup>, Alessandro Paglianti<sup>b</sup>

<sup>a</sup> Dipartimento di Chimica Industriale "Toso Montanari", Alma Mater Studiorum – Università di Bologna  
via Terracini 34 40131 Bologna, Italy

<sup>b</sup> Dipartimento di Ingegneria Civile, Chimica, Ambientale e dei Materiali, Alma Mater Studiorum – Università di Bologna  
via Terracini 34, 40131 Bologna, Italy

\* [antonio.busciglio@unibo.it](mailto:antonio.busciglio@unibo.it)

This paper focuses on the fluid dynamic characteristics of a laboratory scale fully baffled vessel stirred by a Rushton turbine and provided with one inlet and one outlet for the continuous feed of the working liquid. The specific aim of the investigation is the assessment of the operating conditions, namely the agitation speed and the inlet flow rate, at which the influence of feed stream on the overall behavior of the stirred tank starts to be significant from an engineering point of view. Due to the widespread adoption of stirred tanks in continuous industrial processes, the evaluation of the feed effect is expected to provide a useful contribution to evaluate to what extent the current knowledge on batch stirred tanks can be confidently extended to continuous systems. The effect of the inlet jet on the vessel local fluid dynamics is quantified by means of coupled Particle Image Velocimetry (PIV) and Planar Laser Induced Fluorescence (PLIF) measurements, thus resulting in a full characterization of both the flow field and the homogenization dynamics under a number of different operating conditions. The results show that the inlet stream modifies the mean flow field features more importantly the smaller the agitation speed is, as compared with the feed flow rate, i.e. when the ratio between the power input associated to the feed inlet and that provided by the agitator overcomes a critical value. Similarly, a clear dependence of mixing time on inlet flow rate is found, whose entity is larger the smaller the agitation speed is.

### 1. Introduction

Mechanically stirred tanks are widely employed in the process industry for several applications such as blending of liquids (Patel *et al.*, 2013), homogeneous chemical reactions, as well as for many multiphase operations (two- or three- phase chemical reactions, e.g. Montante and Paglianti, 2015; solid suspension, e.g. Tamburini *et al.*, 2012, leaching, liquid-liquid emulsification, gas liquid dispersion, e.g. Scargiali *et al.*, 2015). In industrial processes, stirred vessels are often operated in continuous mode, i.e. with one (or more) fluid inlet and one (or more) fluid outlet steadily operated. When used as chemical reactors in continuous flow mode, this piece of equipment allows higher production rates with respect to batch operations and improved process control (Patel *et al.*, 2014). However, in order to ensure the desired productivity, it is (at least) needed to compare the characteristic, time constant of the reaction of interest with a "fluid-dynamic" time constant. Also, the reactor hydrodynamics has to be carefully considered, in order to avoid malfunctions, which may affect the overall operation performances, due to strong deviations from the ideal perfectly mixed flow as in the cases of short-circuiting, recirculation, dead-volume effects. These effects were quantified in several literature works, see for example Samaras *et al.* (2006), who investigated Newtonian fluid mixing and Patel *et al.* (2013), who studied the effect of continuous operations in continuous stirred vessels filled with non-Newtonian fluids. The hydrodynamics depends in turn on several factors (Aubin *et al.*, 2006): overall flow patterns (vessel and agitator geometry, position and flow rate of inlet and outlet streams), as well as on the local turbulence levels (e.g. determined by agitator geometry and rotational speed). The fluid flow and the associated parameters in batch

stirred vessels have been widely investigated so far, either by experimental characterizations and modelling, while comparatively less information are available for continuous feed conditions.

When referring to mechanically stirred vessels operated in continuous mode, the ratio of batch mixing time  $t_m$  (also referred to as macromixing time) and the mean residence time ( $\tau = V/Q_f$ ) is widely used in practical design (Liu, 2012). Beside, most of the literature investigations on continuous flow stirred tanks deal with the  $\tau/t_m$  ratio (or, in a similar way, the ratio between inlet flow rate and impeller-generated flow rate), suggesting its adoption as the main scale factor (Mavros *et al.* 2002; Samaras *et al.*, 2006; Roussinova and Kresta, 2008). However, inlet/outlet relative geometry may well play a fundamental role in determining the departure from ideal flow at fixed  $\tau/t_m$  ratio (Roussinova and Kresta, 2008) and deeper analysis and more comprehensive methods for the characterization of mixing non-uniformities in continuous flow mixers have been recently proposed (Liu, 2012). Also, the ratio of the impeller to jet momentum  $Mo_{imp}/Mo_{jet}$  has been suggested for evaluating the vessel performances instead of the widely used  $\tau/t_m$  ratio. This parameter was chosen by Torr  *et al.* (2008) to correlate data in semi-baffled stirred reactors in unsteady feed conditions and by Jones *et al.* (2009) in standard, continuously operated stirred vessels. The  $Mo_{imp}/Mo_{jet}$  ratio is allegedly able to better grasp the underlying physics of the interaction between inlet jet and stirred vessel fluid flow. In particular, Jones *et al.* (2009) suggested that larger inlet pipes should be used in case of high flow-rates in order to minimize deviations from ideal mixed flow (decreasing the  $Mo_{jet}$  value), a conclusion similar to that proposed by Aubin *et al.* (2006), who was not however systematically using the jet momentum for data interpretation.

On this basis, the present work is aimed to experimentally measuring the effect of impeller-to-jet momentum ratio  $Mo_{imp}/Mo_{jet}$  on the fluid dynamics of a stirred vessel, by means of a local experimental characterization based on both PLIF and PIV measurement techniques.

## 2. Experimental

The investigated stirred tank consisted of a flat-bottomed cylindrical Plexiglas vessel (diameter,  $T = 0.232$  m, height,  $H = T$ ), equipped with a standard Rushton turbine (diameter,  $D = T/3$ , clearance from vessel bottom,  $C = T/2$ ) and four equally spaced baffles (width,  $W = T/10$ ). The vessel was closed with a lid and entirely filled with the working fluid, that was water.

The inlet and outlet streams were located on the vessel lid through two holes. The inlet hole was placed midway between two subsequent baffles, at a radial distance from the vessel axis,  $R_i = 0.072$  m, ( $R_i/T = 0.31$ ), while the outlet hole was placed at  $120^\circ$  from the former. The outlet hole ( $ID_{outlet} = 0.020$  m) was considerably larger than inlet hole ( $ID_{inlet} = 0.007$ m), in order to minimize the fluid velocity in the outlet region, thus isolating the effect of the inlet jet on the overall fluid dynamics. It was fed and then directly recirculated to the vessel by means of an external peristaltic pump, whose flow-rate was determined by a preliminary calibration. The total volume of the external recirculation loop was equal to  $0.1L$ , that is negligible with respect to the vessel volume. The velocity field and the homogenization time were determined under different combinations of inlet flow rates,  $Q_L$  (0, 4.3, 8.7, 10.5 mL/s) and impeller speeds,  $N$  (50, 100, 150, 300 rpm).

The instrumentation adopted for both PIV and PLIF measurements included a Nd:YAG Litron Laser (light wavelength,  $\lambda = 532$ nm) and a HiSense MkII CCD camera (1344x1024 pixel resolution) provided with a suitable optical filter. A Dantec Dynamics system handled the laser control, the laser/camera synchronisation and the data acquisition. The laser light sheet entered the vessel vertically through lateral walls midway between two subsequent baffles and intercepting the inlet pipe axis. The vessel was placed within a larger square vessel filled with the working liquid in order to minimize optical distortion of the laser light. Further details on the measurement system can be found elsewhere (Montante and Paglianti, 2015).

### 2.1 PIV set up and methods

For the PIV measurements, poly-methyl-methacrylate particles coated with fluorescent Rhodamine-B (mean particle size equal to  $10 \mu\text{m}$ ) were adopted as the fluid seeding. For each experimental condition, after calibration, at least 2000 image pairs were collected (6 image pairs per second), in order to achieve statistic independence of the fluid mean velocities as well as of the turbulent velocity fluctuations. The vertical extension of the measurement zone was limited to  $0.7 T$ , while the radial width included the whole vessel. The time interval between two laser pulses was varied depending on the impeller speed, in order to minimize the measurement errors. A quite common processing route was followed after acquisition: i) cross correlation (interrogation areas  $32 \times 32$  pixels with 50 % overlap, corresponding to a vector resolution of 3 mm); ii) peak validation (first-to-second minimum peak ratio equal to 1.2); iii) range validation (maximum vector length equal to the impeller tip speed,  $V_{tip}$ ); iv) ensemble average of the instantaneous velocity data.

## 2.2 PLIF set up and methods

For PLIF measurement, the mixing dynamics within the vessel was followed by assessing the dispersion of a small amount of aqueous solution of Rhodamine-6G rapidly injected through the inlet tube. Being interested in the time evolution of concentration homogeneity rather than in its absolute value, calibration is not required (Busciglio et al. 2014). In this case, the following processing route was followed: i) image masking, to ensure that the vessel internals do not influence the liquid-phase homogeneity calculation; all subsequent processing should be considered to be applied only to non-masked zones; ii) calculation of the mean intensity image before tracer injection  $Im_i$  (based on the mean of 10 images) and after the achievement of perfect mixing conditions  $Im_f$  (again based on the mean of 10 images); iii) for each instantaneous image, calculation of the intensity deviation image, as:

$$Im_{dev} = \frac{Im_t - Im_i}{Im_f - Im_i} \quad (1)$$

that is a formulation useful to highlight tracer dispersion and discard bias due to laser non-uniformity and inner light reflections; iv) evaluation of the spatial degree of non-homogeneity by means of the image coefficient of variation (CoV), defined as:

$$CoV = \sqrt{\frac{1}{n-1} \sum_{k \in A_p} \left( \frac{Im_{dev,k}}{Im_{dev}} - 1 \right)^2} \quad (2)$$

where the summation is extended to all non-masked pixels of the instantaneous deviation intensity image  $Im_t$ ,  $A_p$ ; v) normalization of the time evolution of image non-homogeneity, computed as:

$$CoV_n = \frac{CoV_t - CoV_f}{CoV_{max} - CoV_f} \quad (3)$$

Where  $CoV_{max}$  and  $CoV_f$  are the CoV values at the injection and after that perfect homogenization is achieved, respectively; vi) calculation of mixing time as the time required to reach  $\sigma_n = 0.05$ , i.e. the time required to complete 95 % of the homogenization process. Selected snapshots collected during the homogenization process are shown in Figure 1.

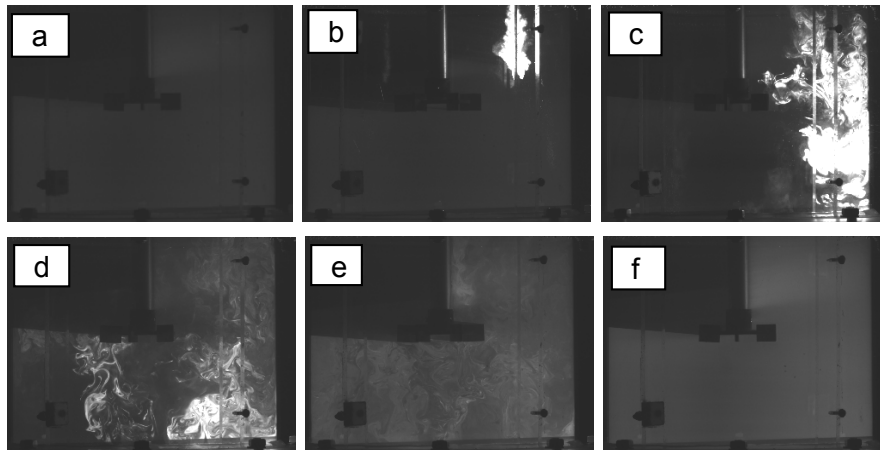


Figure 1: Sequence of raw images as acquired by the PLIF technique at selected time samples starting before the injection until complete homogenization of the tracer, time increasing from a to f.

## 3. PIV data: results and discussion

In Figure 2, the mean dimensionless velocity fields (normalized by  $V_{tip}$ ) as obtained by the PIV measurements for two of the investigated impeller speeds and three feeding rates are shown. As can be observed, for batch operating modes (Figures 2a and 2d), the very well-known double loop discharge flow of the RT is obtained. Also, as expected, the maps of velocity magnitude normalized by  $V_{tip}$  at the two impeller speeds do not coincide, as is the case of fully turbulent conditions, due to the moderate rotational Reynolds number achieved at  $N = 50$  rpm, ( $Re = 5.2 \times 10^3$ ). At the higher impeller speed ( $N = 150$  rpm) the effect of inlet jet on the dimensionless

mean flow field is quite small at both the considered flow rates (Figures 2e and 2f), mainly due to the high momentum associated with the impeller discharge stream. At  $N = 50$  rpm, the effect of the inlet jet is appreciable, although very limited, for  $Q_L = 4.3$  mL/s (Figure 2b), while at the largest feeding rate  $Q = 10.5$  mL/s, a significant modification of the overall mean flow field is obtained (Figure 2c) and the deviation of the impeller discharge flow from the radial direction is apparent.

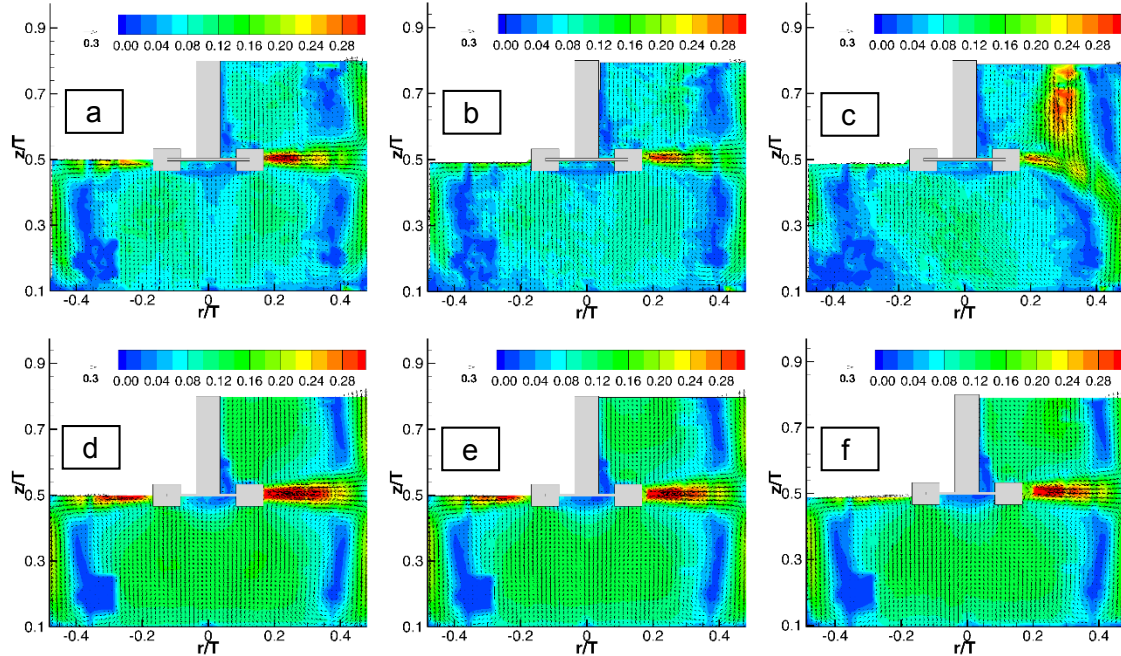


Figure 2: Mean velocity vector plot superimposed to the velocity magnitude normalized by  $V_{tip}$ . (a)  $N = 50$  rpm,  $Q_L = 0$ ; (b)  $N = 50$  rpm,  $Q_L = 4.3$  mL/s; (c)  $N = 50$  rpm,  $Q_L = 10.5$  mL/s; (d)  $N = 150$  rpm,  $Q_L = 0$ ; (e)  $N = 150$  rpm,  $Q_L = 4.3$  mL/s; (f)  $N = 150$  rpm,  $Q_L = 10.5$  mL/s.

The radial profiles of the dimensionless mean radial velocity and the r.m.s. radial velocity fluctuation at the impeller disk plane elevation are shown in Figure 3 for the case of  $N = 50$  rpm for a closer evaluation.

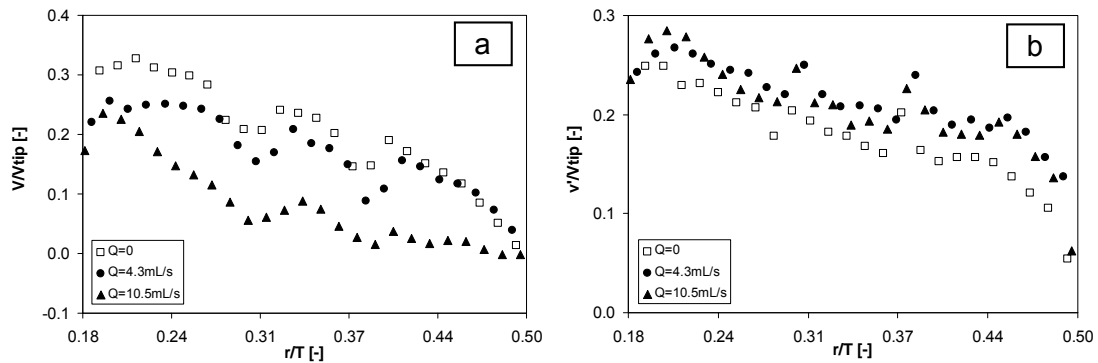


Figure 3: Mean (a) and r.m.s (b) radial velocity at  $z/T = 0.50$  and  $N = 50$  rpm.

The comparison of the profiles obtained under different liquid flow rates clearly highlights that the mean velocity is dampened from the jet action, while the velocity fluctuation is augmented. Based on these results, a closer evaluation of the interaction between the impeller discharge stream and the jet through the calculation of the pumping flow rate will be considered in future investigations, by increasing the vector resolution close to the impeller region.

#### 4. PLIF data: results and discussion

In Figure 4, the time sequence of selected masked deviation images in one measurement condition is reported as an example. The tracer is clearly visible as soon as it enters the vessel. Notably, the impeller discharge stream weakly affects the jet tracer concentration at the beginning of the homogenization process ( $t = 1$  s). The tracer is then directed towards the vessel wall, where it is subsequently dispersed. Clearly, the retention effect in the lower part of the vessel is also due to the relatively low impeller speed. In Figure 5a, the resulting mixing times are reported as a function of inlet flow rate, for different impeller speeds. The effect of inlet flow rate on the mixing time is clear, as expected, because of the increased turbulent dispersion at the jet edges. However, it is worth noting that the mixing time decrease is more important the lower is the impeller speed, as the jet turbulence contribution becomes less important the larger is the power input associated with the impeller. This confirms the use of momentum ratio to scale the measured mixing times, instead of flow-rates ratio, as already suggested by Jones et al. (2009).

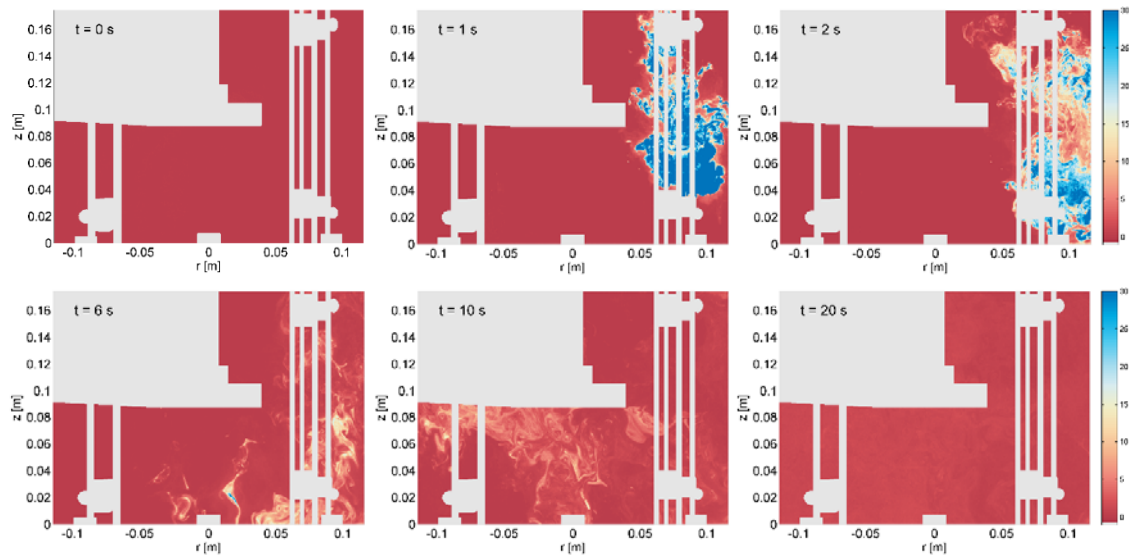


Figure 4: Typical sequence of pixel intensity images during tracer dispersion ( $N = 50$  rpm,  $Q_L = 4.3$  mL/s)

In this case, it was chosen to replace the momentum ratio with the (easiest to calculate) Reynolds ratio:

$$\frac{Mo_{jet}}{Mo_{imp}} = \frac{\rho Q_{jet} V_{jet}}{\rho Q_{imp} V_{imp}} = \frac{Q_{jet} V_{jet}}{N_Q (ND^3)(ND)} = \frac{1}{N_Q} \frac{Q_{jet} V_{jet}}{N^2 D^4} \quad (4)$$

$$\frac{Re_{jet}}{Re_{imp}} = \frac{\rho D_{jet} V_{jet}}{\mu} \frac{\mu}{\rho N D^2} \propto \frac{(Q_{jet} V_{jet})^{1/2}}{N D^2} \propto \left( \frac{Mo_{jet}}{Mo_{imp}} \right)^{1/2} \quad (5)$$

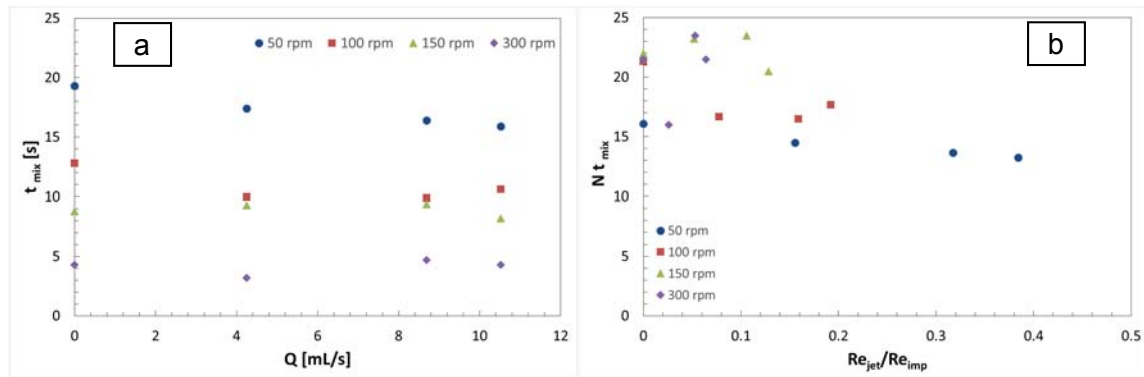


Figure 5: (a) Tracer homogenization time as a function of inlet flowrate; (b) dimensionless mixing time as a function of the jet-to-impeller Reynolds ratio.

Even if momentum ratio has a clearer physical meaning than the relevant Reynolds ratio, its ease of use makes it a good candidate to obtain useful scaling relation. When reporting dimensionless mixing times  $Nt_m$  as a function of the aforementioned Reynolds ratio, data show a slight decreasing trend, as can be observed in Figure 5b. However, some scatter is evident, but this may be partly due to the uncertainties associated with the mixing times measurements. Data taken at 50 rpm show smaller dimensionless mixing time, as expected because of not fully developed turbulent regime, but a clearly decreasing trend is observed. It is worth notice that the consumed power for the inlet flow rate is negligible if compared with the power due to the impeller, indeed the ratio between the former and the latter power is always lower than 1%.

## 5. Conclusions

The experimental data collected in this work have confirmed that the presence of a jet inlet can significantly modify the flow patterns inside a stirred tank. When the power dissipated by the inlet feed,  $P_j$ , is negligible with respect to the power consumed by the impeller,  $P_i$ , the flow pattern does not exhibit significant variations with respect to batch conditions, while important differences are observed as soon as the power  $P_j$  reaches the value of about 1% of  $P_i$ . Also, the inlet feed in a continuous stirred tank reactor can improve the mixing process. The comparison of our results with the limited experimental works available so far clearly shows that the effect of the jet could be positive or negative, depending on the position of the inlet/outlet pipes adopted for the feed and the outflow. The velocity fields and the homogenization time collected in this work show that the effect of the feed cannot be neglected, especially when the impeller speed is low as in the case of bioreactors. In these cases, the position and the size of the inlet and outlet pipes have to be carefully selected, because proper choice could improve the mixing process while a wrong choice could induce the increment of the time necessary for obtaining the full homogenization of the reactor.

## Acknowledgements

The financial support of MIUR "Progetto SO.F.I.A. CTN01\_00230\_450760- Sostenibilità della filiera agroalimentare italiana" is gratefully acknowledged.

## References

- Aubin J., Kresta S.M., Bertrand J., Xuereb C., Fletcher D.F., 2006, Alternate operating methods for improving the performance of continuous stirred tank reactors, *Chem. Eng. Res. Des.* 84(A7), 569-582.
- Busciglio A., Grisafi F., Scargiali F., Brucato A., 2014, Mixing dynamics in uncovered unbaffled stirred tanks, *Chem. Eng. J.*, 254, 210-219.
- Jones P.N., Ozcan-Taskin N.G., Yianneskis M., 2009, The use of momentum ratio to evaluate the performance of CSTRs, *Chem. Eng. Res. Des.*, 87, 485-491.
- Liu M., 2012, Age distribution and the degree of mixing in continuous flow stirred tank reactors, *Chem. Eng. Sci.*, 69, 382-393.
- Mavros P., Xuereb C., Fort I., Bertrand J., 2002, Investigation by laser Doppler velocimetry of the effects of liquid flow rates and feed positions on the flow patterns induced in a stirred tank by an axial-flow impeller, *Chem. Eng. Sci.*, 57, 3939-3952.
- Montante G., Paglianti A., 2015, Fluid dynamics characterization of a stirred model bio-methanation digester, *Chem. Eng. Res. Des.*, 93, 38-47.
- Patel D., Ein-Mozaffari F., Mehrvar M., 2013, Characterization of the continuous flow mixing of non-Newtonian fluids using the ratio of residence time to batch mixing time, *Chem. Eng. Res. Des.*, 91, 1223-1234.
- Patel, D., Ein-Mozaffari, F., Mehrvar, M., 2014, Using tomography to visualize the continuous-flow mixing of biopolymer solutions inside a stirred tank reactor *Chem. Eng. J.*, 239, 257-273.
- Roussinova V., Kresta S.M., 2008, Comparison of continuous blend time and residence time distribution models for a stirred tank, *Ind. Eng. Chem. Res.*, 47, 3532-3539.
- Samaras K., Mavros P., Zamboulis D., 2006, Effect of continuous feed stream and agitator type of CFSTR mixing state, *Ind. Eng. Chem. Res.*, 45, 4805-4815.
- Scargiali F., Busciglio A., Grisafi F., Brucato A., 2013, Influence of viscosity on mass transfer performances of unbaffled stirred vessels, *Chem. Eng. Trans.*, 32:1483-1488, DOI: 10.3303/CET1332248
- Tamburini A., Cipollina A., Micale G., Brucato A., 2012, Measurements of  $N_{js}$  and power requirements in unbaffled bioslurry reactors, *Chem. Eng. Trans.*, 27:343-348, DOI: 10.3303/CET1227058
- Torré J.-P., Fletcher D.F., Lasuye T., Xuereb C., 2008, An experimental and CFD study of liquid jet injection into a partially baffled mixing vessel: a contribution to process safety by improving the quenching of runaway reactions, *Chem. Eng. Sci.*, 63, 924-942.